

REVIEW ARTICLE

Predator–prey encounter and capture rates in turbulent environmentsH. L. Pécseli,¹ J. K. Trulsen,² and Ø. Fiksen³**Abstract**

Predator–prey encounter and capture rates are key drivers of population dynamics of planktonic organisms. Turbulent mixing gives rise to enhanced encounter rates, but high turbulence levels may reduce capture rates. We present an estimate for the optimum turbulence level for a predator that is characterized by a number of parameters, such as its range of interception. A limit at small spatial scales is recovered where classical diffusion competes with turbulent motions. Particular attention is given to the question of turbulence-induced noise signals, which a predator can misinterpret as indicators of prey. Analytical expressions are obtained for the occurrence of these “error signals” in terms of the basic parameters of the problem. The basic hypothesis rests on the assumption that if several such error signals are received within a time needed for the predator to capture prey, then its capacity for capturing prey is reduced or even made impossible. The aim of the study is to present closed general analytical expressions for the capture rate in turbulent environments, where the results contain free parameters that can be used for modeling selected species. Statistical descriptions of the velocity fluctuations on spatial scales in the viscous subrange of turbulence are determined and placed in the context of predator–prey encounter and capture rates. The relevant probability densities are obtained by direct numerical solutions of the Navier–Stokes equation for turbulent conditions. The analysis is given a compact formulation in terms of scaled dimensionless variables.

Keywords: inertial and viscous subranges of turbulence, signals and noise, numerical simulations, universal scaling laws

Introduction

[1] Encounter and capture rates are key drivers of growth, predation, and population dynamics of planktonic organisms (Kjørboe 2008). For aquatic organisms in the millimeter size range, both processes are sensitive to random or turbulent motions in ambient fluid (Rothschild and Osborn 1988; MacKenzie et al. 1994; Osborn 1996). A number of observations support the idea that turbulence has a detectable influence on the feeding rate of plankton

(Sundby and Fossum 1990; Saiz and Alcaraz 1991, 1992a). Consequently, there has been a continued interest in quantifying and modeling the linkages between small-scale turbulence in the ocean and ecosystem structure or productivity of commercial species and their food sources (Barange et al. 2010).

[2] Encounter and capture processes depend on organism-specific traits and properties, such as sensory abilities and modes, behaviors, and adaptive trade-offs (Fiksen et al. 1998;

¹Department of Physics, University of Oslo, NO-0316 Oslo, Norway

²Institute for Theoretical Astrophysics, University of Oslo, NO-0315 Oslo, Norway

³Department of Biology, University of Bergen, NO-5020 and the Hjort Centre for Marine Ecosystem Dynamics, Bergen, Norway

Correspondence to
Hans L. Pécseli,
hans.pecseli@fys.uio.no

Kjørboe et al. 2010; Kjørboe 2011). Models therefore need to be flexible and include the relevant biological and physical parameters. Another issue is to define the scale at which active propulsion and behavior diminish the role of turbulence, for instance, the size of larval fish (Kjørboe and MacKenzie 1995; MacKenzie and Kjørboe 1995), and in the other end, the scale where viscosity takes over and diffusion is the main driver of particle flux at the size of the largest phytoplankton (Karp-Boss et al. 1996; Jumars et al. 2009).

[3] Many models of turbulence and interactions with the plankton have been developed (Rothschild and Osborn 1988; MacKenzie et al. 1994; Osborn 1996). Here we first review and extend some of our own results (Mann et al. 2005; Pécseli and Trulsen 2007; Pécseli et al. 2012) to arrive at analytical models and test their predictive ability with explicit numerical simulations and experiments. The correspondence between the data and the models is strong, adding confidence to the analytical formulations.

[4] Then we proceed to analyze another issue in how turbulence challenges aquatic organisms. Many plankton use hydrodynamic signals and deformation rates generated by moving prey for detecting their presence and exact location for capture (Visser 2001). These signals can be blurred by turbulence, since turbulent velocity differences may be difficult to separate from those generated by moving prey, such that prey capture success decreases at high turbulence (Saiz and Kjørboe 1995). Consequently, turbulence increases prey encounter rates but decreases capture success, and the total benefit of turbulence is therefore believed to be “dome shaped,” with an optimum at intermediate levels (MacKenzie et al. 1994; MacKenzie and Kjørboe 2000). In the field this is believed to result in active habitat selection by plankton organisms, most often moving to a deeper location at stronger wind and mixing levels to maintain optimum levels of turbulence (Incze et al. 2001; Visser et al. 2001). Other explanations exist for this phenomenon, such as passive mixing (Heath et al. 1988) and a turbulence-related trade-off between foraging and predation risk (Visser et al. 2009).

[5] Earlier treatments of the “downside of turbulence” have included an assumption that the predator will have to respond to a well-defined disturbance induced by prey, with a single threshold value as a detection criterion (Kjørboe and Saiz 1995). We consider these types of models in detail and find that a proper description of the turbulent velocity variations over the antennae of a predator requires a more detailed analysis, leading to results that cannot readily be expressed in terms of a simple threshold for detection.

[6] The analysis is formulated in terms of a few characteristic parameters, combined into scaled dimensionless variables. Flow (i.e., the water) is characterized by its kinematic viscosity ν , turbulence by the specific energy dissipation rate ε , and plankton by its capture range R and opening angle θ in its field of reception. An illustration of the present definition of θ is given by Pécseli and Trulsen (2007). Predators and prey can have a self-induced motion. The minimum time needed for capturing prey is given as a time constant $\Delta\tau$. Several studies show that on detecting a potential prey organism in their vicinity, both fish larvae and large copepods initiate what can be termed a pursuit-attack phase (Caparroy et al. 2000; Kjørboe 2013). The pursuit consists of swimming or jumping rapidly (sometimes with speeds exceeding $U_j \approx 30 \text{ mm s}^{-1}$) toward the prey until they get close enough to initiate an attack by either sucking it into their jaws or grabbing it with their appendages. If the range of detecting prey is R , we can estimate a minimum time as U_j/R . Taking as an example $R \approx 10 \text{ mm}$ and the velocity estimate quoted before, we have for this case a minimum time of 0.3 s for capture. To estimate $\Delta\tau$, we add time to identify prey and to change orientation prior to attack, and we expect $\Delta\tau$ of 0.5–1 s to be representative.

[7] With information on $\Delta\tau$, possibly with added characteristic velocities for predator and for prey, we can predict an encounter rate and a capture probability in terms of known constants and an empirically determined analytical expression for the probability density of transit times. In particular, an optimum turbulence level can be predicted. Considering

individual capture processes, several other parameters can be important (relative orientations of predator and prey, etc.), but the selected parameters considered in the models are universal and relevant for all plankton. The results are presented in the form of figures where parameters relevant for a particular problem can be used. The applicability of these results is facilitated by the use of normalized units that combine several parameters. The results are expressed in terms of normalized (or “scaled”) dimensionless combinations of variables. This choice allows compact analytical expressions and facilitates simple representations of figures.

[8] Our analysis gives particular attention to analytical models that can account for the time variability of signals detected by predators. Signals originating from moving prey and from random motions in the surrounding water are in principle indistinguishable, and differences need to be described and characterized in terms of probabilities for magnitudes of the perturbations and their time durations. The results thus provide some useful tools in characterizing turbulent fluctuations as they are observed by plankton on the relevant small scales in the viscous subrange. Our results indicate that the viscous subrange is particularly important for aquatic microorganisms. This subrange has not been studied in the same detail as the inertial subrange of turbulence.

Model Description

[9] Considering planktonic predator-prey encounter and capture rates in turbulent aquatic environments, we take the capture rate, that is, the part of the total flux being captured, to be the product of prey encounter rate J_∞ and capture probability $P_c(c)$:

$$J_{\text{cap}} = J_\infty P_c(c), \quad (1)$$

where $P_c(c)$ measures the fraction of successful encounters. All quantities entering are to be understood as averages. The seemingly simple result in Eq. 1 implies that the average of the product of encounter and ensuing capture is taken to be a product of the two averages. This can be correct only if encounter and capture are

independent. This is, strictly speaking, not the case: encounter probabilities are proportional to local prey density. Since capture influences prey density, the stated independence cannot strictly be argued, but we found by numerical simulations that Eq. 1 serves as a good approximation. One reason for this is that the Kolmogorov constant C_K , which serves as the basic parameter for all studies related to turbulence in the inertial subrange, is known only with some uncertainty. In particular, C_K enters analytical results for J_∞ . It turns out that the uncertainty on C_K dominates possible uncertainties in the approximations inherent in taking the product in Eq. 1.

[10] From the capture probability we can derive a simple result for the prey escape probability as $1 - P_c(c)$; thus, the probability for passively moving prey to escape capture is solely due to turbulent motions in the flow.

[11] The independence assumption in Eq. 1 has the consequence that encounter and capture rates can be analyzed independently. We use a combination of analytical and numerical methods. When formulated for individual ranges of the turbulence scales, the problems contain only a few parameters, and we found that dimensional reasoning in terms of the Buckingham Π -theorem (Buckingham 1914) offers a valuable tool for obtaining the proper scaling of the results in terms of the relevant parameters. The numerical results are based on data from direct solutions of the Navier–Stokes equation (Biferale et al. 2004, 2005, 2006).

[12] We begin with a review of previous results together with a number of figures that illustrate their basic features. A basic assumption of the analysis is that a range of interception R of a predator can be uniquely defined. We then discuss limitations in this assumption and analytical methods for quantifying disturbances from the turbulent environment that a predator can interpret as a false signal of the presence of prey. Similarly, prey can interpret such disturbances as false evidence of a predator. In the first case, a predator can attack even in absence of prey, while in the latter case, prey can be seen to perform escape responses in the absence of a predator.

Results

[13] The results from the analysis are separated into two parts, encounter and capture. Both depend on the range of interception R characterizing the predator, as well as other parameters to be specified. We can have R in the inertial range or in the viscous subrange of turbulence. In addition we also identify a “Brownian subrange” where thermal fluctuations have a role: this limit can be relevant for organisms in the 100- μm size range. Previous results are presented as a review and to serve as a frame of reference for new results.

Summary of Results for Different Subranges

[14] The separation between the inertial and viscous subranges is defined as the length scale η_0 , where the longitudinal second-order velocity structure function for the viscous subrange equals the corresponding Kolmogorov–Obukhov structure function for the inertial subrange (Davidson 2004). In terms of the Kolmogorov length scale $\eta \equiv (\nu^3/\varepsilon)^{1/4}$, we find $\eta_0 \equiv (15C_K)^{3/4}(\nu^3/\varepsilon)^{1/4} \approx 13\eta$, where the numerical constant is derived from the empirically obtained Kolmogorov constant $C_K = 2.1–2.5$ and the corresponding coefficient $C_\nu = 1/15$ for the viscous subrange that is known from analysis. The difference between η and η_0 is not trivial. The Kolmogorov time scale is defined as $\tau_K \equiv \sqrt{\nu/\varepsilon}$.

Encounters: Inertial Subrange

[15] First, ignoring self-induced motions of predators and prey, the encounter rate due to turbulent motions in the flow for spherical interception volumes (with radii R in the inertial subrange, $R > \eta_0$) is

$$\frac{J_\infty^{(i)}}{n_0} = C_M R^{7/3} \varepsilon^{1/3}, \quad (2)$$

where n_0 is the reference prey concentration in an unperturbed environment, and $C_M \approx 6$ is a universal constant obtained empirically. By the superscript (i) we indicate the inertial subrange of the turbulence. The scaling law Eq. 2 for the inertial subrange can be found by solving a model diffusion equation (Rothschild and Osborn 1988; Osborn 1996), but the result can also be obtained by dimensional reasoning without

reference to any model equation (Mann et al. 2005; Pécseli and Trulsen 2007). Results from laboratory experiments (Mann et al. 2005) and numerical simulations (Pécseli and Trulsen 2007) provide support for Eq. 2.

Encounters: Viscous Subrange

[16] For $R < \eta_0$ we find

$$\frac{J_\infty^{(v)}}{n_0} = C_V R^3 \sqrt{\varepsilon/\nu}, \quad (3)$$

where $C_V \approx 1.1$ is a universal constant obtained empirically, while n_0 is the reference prey concentration from Eq. 2. By the superscript (v) on J_∞ we indicate the viscous subrange of the turbulence. Numerical results covering both the inertial and viscous subranges are shown in Fig. 1, where symbols refer to different opening angles θ in a conical volume of interception. The agreement is satisfactory.

Encounters: Brownian Diffusion Range

[17] It has been argued that turbulent motions can be effective even for scales as small as 10–100 μm (Barton et al. 2013). The smallest scale recognized by the classical analysis of turbulence in incompressible neutral fluids is the Kolmogorov microscale η . For very small scales (much smaller than η), the result

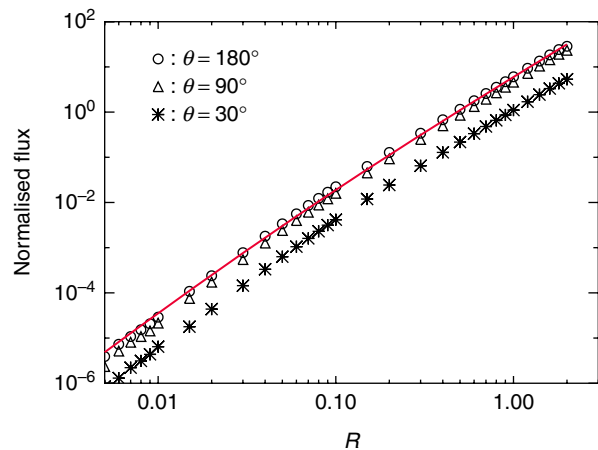


Fig. 1 Numerically obtained asymptotic prey fluxes to a predator with a conical field of view with opening angle θ . The view directions with respect to the local flow velocity vector are uniformly distributed over 4π . The solid red line gives the model fit for the spherical case covering both Eqs. 2 and 3. The results are shown for varying range of interception, R .

Eq. 3 indicates that the encounter rate vanishes at R^3 , implying that there should be no detectable relative motion on scales much less than η . In reality, however, there will always be *some* fluctuations due to finite temperature; for instance, for aerosols in the atmosphere these motions contribute to the coagulation of small particles into larger ones.

[18] The question obviously arises, then, at what size turbulent transport is more important than molecular, or Brownian, diffusion. The answer can readily be found by comparing the turbulent flux to an absorbing surface with what is found for molecular Brownian diffusion. We obtain the nutrient flux $J^{(B)}$ due to Brownian motion to a spherical absorbing surface with radius R by solving the diffusion equation in spherical geometry with a constant diffusion coefficient D . The spherical surface with radius R here models the organism. The diffusion coefficient D is related to the thermal motions by the fluctuation dissipation theorem (Chandrasekhar 1954; Pécseli 2000). With the given simplified symmetry, the ∇^2 operator can be expressed in a convenient form (Chandrasekhar 1954) to give

$$\frac{\partial(rn)}{\partial t} = D \frac{\partial^2(rn)}{\partial r^2}, \quad (4)$$

where n is the nutrient concentration and r is the radial distance variable. We impose the fast absorbing boundary condition $n(r=R)=0$ for $t>0$, while $n(r\rightarrow\infty)=n_0$. This problem has an exact analytical solution, where only the time asymptotic limit is relevant here (Chandrasekhar 1954; Pécseli 2000). The net diffusion flux to the spherical surface is then $J^{(B)}=4\pi DRn_0$, where it is implicitly assumed that the absorbing surface is large and at rest, so that it does not itself participate in the Brownian motion. With n representing the concentration of nutrition or prey, then $J^{(B)}$ represents the predators encounter rate with prey for the case where the motion is solely Brownian.

[19] For the length scales relevant here, we use the result for the turbulent flux in the viscous subrange $J_0 \approx C_V n_0 R^3 \sqrt{\varepsilon/\nu}$. The limiting length scale R_ℓ where

the Brownian flux equals the turbulent flux is then

$$R_\ell \approx \left(\frac{16\pi^2}{C_V^2}\right)^{1/4} \left(\frac{D^2\nu}{\varepsilon}\right)^{1/4} \approx 3.4 \frac{\eta}{\sqrt{Sc}}, \quad (5)$$

in terms of the Schmidt number $Sc \equiv \nu/D$, where η/\sqrt{Sc} is known as the “Batchelor scale” (Batchelor 1959). The flux due to Brownian motion will dominate if $R < R_\ell$. This result will apply for turbulent incompressible flows, in particular, and also for turbulent transport in the atmosphere when the conditions can be taken to be locally homogeneous and isotropic. It is not obvious which value of the diffusion coefficient D applies here. In the case of finite-sized particles arriving at the absorbing surface, the classical expression for the diffusion coefficient is $D \approx \kappa T/(6\pi a\mu)$ for a particle with radius a at a temperature T , where the dynamic viscosity is μ and κ is Boltzmann’s constant (Chandrasekhar 1954). Here we use the molecular diffusion values for estimates, which can serve as approximations for nutrients dissolved in the water (Schroeder 2000). At room temperature in water we have $D \approx 10^{-5} - 10^{-4} \text{ mm}^2 \text{ s}^{-1}$, while typical values for air can be $D \approx 10 \text{ mm}^2 \text{ s}^{-1}$. For water (with kinematic viscosity $\nu = 0.89 \text{ mm}^2 \text{ s}^{-1}$), for instance, we then have $R_\ell \approx 10^{-3} \varepsilon^{-1/4} \text{ mm}$ when ε is inserted in units of millimeters squared per second cubed, giving $R_\ell \approx 5 \times 10^{-2} \text{ mm}$ for $\varepsilon \approx 1 \text{ mm}^2 \text{ s}^{-3}$. The turbulence level chosen here is found in nature in turbulent coastal zones (Granata and Dickey 1991), so we can argue that turbulence can be important in nature also for scales down to $100 \mu\text{m}$, at least compared with Brownian motion. For the general case, the proper value of the relevant diffusion coefficient is to be inserted into the analytical expression for R_ℓ .

[20] Below we will give results allowing estimates of relative velocity variations due to turbulence on the smallest scales; see “Capture with Varying Turbulence Intensity”. Table 1 summarizes turbulence parameters found in nature. Fluid dynamics in the limit where Brownian motions are important on the same level as turbulent diffusion is poorly understood, in general.

Table 1 Typical turbulence parameters encountered in natural turbulent flows [Granata and Dickey 1991; Kiørboe and Saiz 1995]. The kinematic viscosity of water is taken to be $\nu = 0.89 \text{ mm}^2 \text{ s}^{-1}$.

Location	Specific energy dissipation rate, ε	Modified Kolmogorov length, η_0	Kolmogorov time, $\tau_K \equiv \sqrt{\nu/\varepsilon}$
Open ocean	$\sim 10^{-4}$ to $1 \text{ mm}^2 \text{ s}^{-3}$	~ 130 – 13 mm	~ 100 – 1 s
Shelf	$\sim 10^{-1}$ to $1 \text{ mm}^2 \text{ s}^{-3}$	~ 26 – 13 mm	~ 3.0 – 1 s
Coastal zone	$\sim 10^{-1}$ to $10^2 \text{ mm}^2 \text{ s}^{-3}$	~ 26 – 2.6 mm	~ 3.0 – 0.1 s
Tidal front	$\sim 10 \text{ mm}^2 \text{ s}^{-3}$	$\sim 6.5 \text{ mm}$	$\sim 0.3 \text{ s}$

Self-Induced Motions

[21] The foregoing results were obtained by ignoring self-induced motions of plankton. Some experiments have demonstrated that the observed encounter rates could best be explained by including self-induced predator motions (Zilman et al. 2013). Numerical simulations (Pécseli et al. 2010) have demonstrated that the encounter rate given as

$$J_\infty = n_0 \sqrt{\left(J_\infty^{(i,v)}\right)^2 + (\pi R^2 U_c)^2} \quad (6)$$

serves as a good or even excellent approximation for a predator moving with a constant self-induced velocity U_c with respect to the local fluid element. The result can be used for both inertial and viscous subranges with the proper expressions for $J_\infty^{(i)}$ or $J_\infty^{(v)}$ inserted. For cruising as well as spiraling motions (Visser and Kiørboe 2006), we can apply Eq. 6 with good accuracy: because of the disturbance of trajectories caused by the turbulent motions, the difference between cruising and spiraling motions is not significant. A correction for the opening angle of the field of view of the predator can be included as well (Pécseli et al. 2010): as it stands, the expression in Eq. 6 assumes spherical views.

[22] As mentioned, Eq. 6 is conditional in the sense that it takes the predator velocity to be constant. For cases where U_c is statistically distributed, it makes a nontrivial difference whether we average J_∞ as given by Eq. 6 or average J_∞^2 and then take the square root for estimating the average encounter rate.

[23] The result Eq. 6 can be generalized by allowing for random motions of both predators and prey (Rothschild and Osborn 1988). By denoting the average of these predator/prey motions by an overbar, we find a

somewhat more general result:

$$\sqrt{J_\infty^2} = n_0 \sqrt{\left(J_\infty^{(i,v)}\right)^2 + (\pi R^2)^2 (\overline{U_c^2} + \overline{U_p^2})}, \quad (7)$$

where the velocity U_c refers to the predator motions, and U_p to prey motions. The angles between the vector directions of U_c and U_p are assumed to be uniformly distributed over 4π . The average is to be interpreted as an ensemble average at asymptotic times after release. A more detailed discussion is given by Evans (1989). Compared with the results of, for instance, Rothschild and Osborn (1988), Eq. 7 gives the correct encounter rate caused by turbulent mixing when both predator and prey are at rest in the local fluid volume. Numerical tests of Eq. 6 (Pécseli et al. 2010) can be interpreted as also relevant for Eq. 7, where either $\overline{U_c^2}$ or $\overline{U_p^2}$ is set to zero. Trajectory distortions by turbulent motions implied only small changes in the encounter rate for different strategies of motion (corresponding to linear or spiraling motion with respect to the local flow element), as long as $U_c \leq J_\infty/R^2$. Also, the effects of changes in orientation have been analyzed (Mann et al. 2006). The reference and realistic case is one where the predator is oriented randomly with respect to the local flow velocity vector. The encounter rate could be increased by up to 20% if the predator had an ability to orient itself with respect to the local flow, although no optimum strategy could be prescribed. Travel-pause predators were also studied (Pécseli et al. 2010), resulting in estimates for some optimum strategies.

Captures

[24] While turbulence can be an advantage by increasing encounter rates, it might also have adverse effects by

reducing the capture rates (MacKenzie et al. 1994). In some cases the latter effects might even be anticipated to dominate for all turbulence levels (Urtizberea and Fiksen 2013). Irrespective of the other merits of the pioneering paper by MacKenzie et al. (1994), it contains a basic error by stating that the separation between two points moving in a turbulent flow increases linearly with time. It is not so: it is the well-known problem of relative motion (Richardson 1926), with the particle separation proportional to εt^3 , where ε is the specific energy dissipation of the turbulence. We solve the problem in terms of transit times with an experimentally estimated universal transit time probability density.

[25] Returning to Eq. 1, we discuss the capture rate given an encounter. The fraction of successful encounters, $P_c(c)$, depends on a number of physical parameters. The time τ available for capture, given an encounter, is a universal parameter (MacKenzie et al. 1994; Pécseli et al. 2012), and we concentrate on this. The prey transit time through the volume of interception is statistically distributed, with distributions that can be obtained experimentally (Mann et al. 2003) or numerically (Pécseli and Trulsen 2010). The simplest model for capture assumes that the predator needs some finite time $\Delta\tau$ for capturing prey. If the time available is less than this, there will be no capture; if the time is greater, we assume capture with certainty. More detailed models with more adjustable parameters have been suggested (Pécseli et al. 2012), but given the uncertainties in experimental data, we assume that the simple model outlined here will suffice. We thus assume that the probability of capture for given transit time τ is a unit step function $S(c|\tau) = \mathcal{H}(\tau - \Delta\tau)$, where \mathcal{H} is Heaviside's unit step function. The result will demonstrate the trend, while a more detailed model can be implemented for specific organisms.

[26] Given estimates for transit time probability densities $P_\tau(\tau)$, we have $P_c(c) = \int_0^\infty S(c|\tau) P_\tau(\tau) d\tau = \int_{\Delta\tau}^\infty P_\tau(\tau) d\tau$. With the present simple model, we thus find that the capture probability is given simply as 1 minus the cumulative probability distribution $\int_0^{\Delta\tau} P_\tau(\tau) d\tau$ of transit times τ .

[27] We distinguish two subranges for the distribution of transit times: inertial and viscous. The two relevant probability densities will have different forms,

involving different scalings of the relevant variables. The scaling in terms of the parameters of the problem can be determined analytically by dimensional arguments, while the universal functional form is established by fitting analytical expressions with a number of free parameters to data obtained by numerical or laboratory experimental results.

Capture Probabilities: Inertial Subrange

[28] By dimensional arguments we find that the probability density for transit times through a given volume must have the form

$$P_\tau(\tau) = \frac{\varepsilon^{1/3}}{R^{2/3}} F_1\left(\tau \frac{\varepsilon^{1/3}}{R^{2/3}}\right), \quad (8)$$

with F_1 being a dimensionless function of one dimensionless scaled variable. The universal functional form F_1 can be obtained by a fit to experimentally or numerically obtained data. R is here a characteristic length scale determining the volume, for instance, the radius of a spherical capture volume. Fig. 2 shows results for the

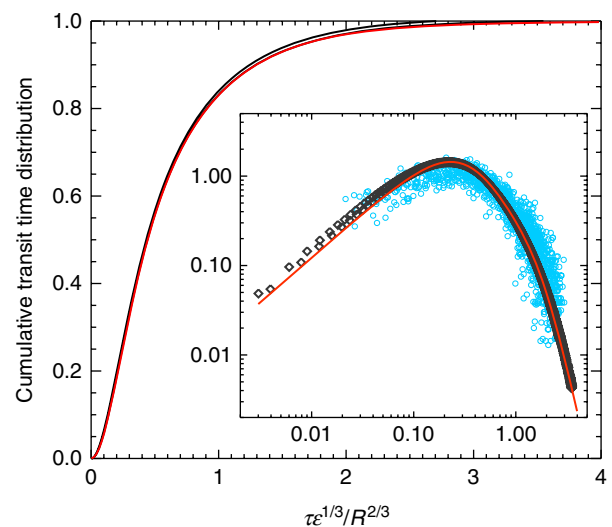


Fig. 2 Analytical model for the cumulative transit time distribution for spherical interception volumes with radii R in the inertial subrange. The inset shows the probability density of transit times τ , given here as a function of the dimensionless variable $\tau\varepsilon^{1/3}/R^{2/3}$, where ε is the energy dissipation rate per unit mass (see Eq. 8). Data are from numerical simulations (black diamonds; Pécseli and Trulsen 2010) and an independent laboratory experiment (blue circles; Mann et al. 2003). The use of dimensionless variables allows the results to be presented in terms of one universal curve.

transit time probability density, as well as the cumulative probability density, relevant for R in the inertial sub-range of turbulence.

Capture Probabilities: Viscous Subrange

[29] Again by dimensional arguments, we found a scaling for the transit time probability density appropriate for the viscous subrange in the form

$$P_\tau(\tau) = \sqrt{\frac{\varepsilon}{\nu}} F_2 \left(\tau \sqrt{\frac{\varepsilon}{\nu}} \right) \quad (9)$$

that is independent of R . Here we have another dimensionless function F_2 that, like F_1 , is also determined by fitting data from numerical simulations (Pécseli et al. 2012). The fits for the cumulative probability have the analytical form $1 - 1/(1 + a[1]x + a[2]x^2 + a[3]x^3 + a[4]x^4)$, where we obtain different sets of coefficients $a[j]$, $j = 1, 2, 3, 4$, for the viscous as well as for the inertial subranges. The coefficients depend also on the form of the capture volume. These coefficients are universal for the conditions specified.

Results for Inertial and Viscous Subranges

[30] With the simple capture probability model discussed before, assuming no capture for $t < \Delta\tau$ and capture with certainty for $t \geq \Delta\tau$, we find the closed expression for the capture rates for R in the inertial subrange in the form

$$J_{\text{cap}} = \frac{C_M n_0 \varepsilon^{1/3} R^{7/3} \chi(\theta)}{1 + \sum_{j=1}^4 a[j] (\Delta\tau \varepsilon^{1/3} / R^{2/3})^j} \quad (10)$$

Note that Eq. 10 can be described in terms of one scaled variable $\Delta\tau \varepsilon^{1/3} / R^{2/3}$ with the capture range normalized as $J_{\text{cap}} \Delta\tau / (n_0 R^3)$. For the viscous subrange we find similarly that

$$J_{\text{cap}} = \frac{C_V n_0 R^3 \chi(\theta) \sqrt{\varepsilon/\nu}}{1 + \sum_{j=1}^4 b[j] (\Delta\tau \sqrt{\varepsilon/\nu})^j} \quad (11)$$

where all numerical coefficients $a[j]$ and $b[j]$ for $j = 1, 2, 3, 4$ are obtained as discussed before, with tables given elsewhere (Pécseli et al. 2012). A correction factor $\chi(\theta)$ is introduced in both Eqs. 10 and 11 to account for different opening angles of a conical field of view

(Pécseli et al. 2012). Also, the coefficients $a[j]$ and $b[j]$ have to be chosen accordingly. The use of dimensionless variables allows a particularly compact formulation of the results in Eqs. 10 and 11.

[31] Results for J_{cap} with R in the inertial subrange as in Eq. 10 are summarized in Fig. 3 for a hemispherical shape for the capture volume (i.e., $\theta = 90^\circ$). This particular opening angle has been suggested as particularly relevant (Lewis and Pedley 2001; Lewis 2003; Lewis and Bala 2006). We find a characteristic dome-shaped capture rate as illustrated in Fig. 3, with an optimum turbulence level (MacKenzie et al. 1994), in our case at $\varepsilon \approx 0.35R^2/\Delta\tau^3$, for a predator characterized by a hemispherical volume of interception. Taking as an example a passively moving predator with $R = 10$ mm and $\Delta\tau = 2$ s, we have the optimum at $\varepsilon \approx 4$ mm² s⁻¹, a value often found in the coastal zones (Granata and Dickey 1991; Kiørboe and Saiz 1995). Stronger

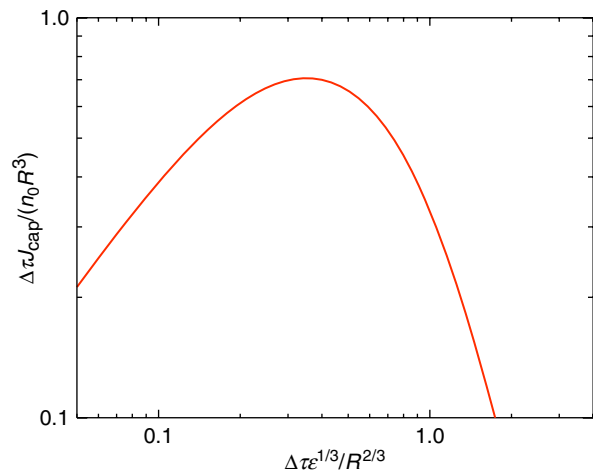


Fig. 3 Results for the net captured prey flux shown in double logarithmic presentation for varying parameters, where $\Delta\tau$ is the minimum time needed for capture, R is the capture range, ε is the specific energy dissipation rate of the turbulence (dissipated energy per mass unit), and n_0 is the reference prey concentration at large distances from the predator. The result is obtained by Eq. 10. The present model assumes a hemispherical capture volume with a radius R in the inertial turbulence subrange. For small values of $\Delta\tau \varepsilon^{1/3} / R^{2/3}$ the captured flux increases due to turbulence-induced encounter rates, whereas for large values the flux decreases due to short times available for capture, that is, short transit times through the volume of interception, which reduces capture rates. The figure also illustrates the advantage of using dimensionless normalized variables: had we presented J_{cap} as a function of, for example, $\Delta\tau$ alone, we would need separate curves for each value of R and ε . To use the present form we combine the actual values of the parameters to give $\Delta\tau \varepsilon^{1/3} / R^{2/3}$ and then use the red curve to obtain the corresponding J_{cap} value.

turbulence, as found in the tidal front, will be disadvantageous for a predator with these characteristics.

[32] The model illustrated in Fig. 3 is simple yet useful for an estimate. A more generally applicable result contains two time scales that can be adjusted for different species (Pécseli et al. 2012) and allows for modeling a gradually varying capture probability, replacing the simple step model used in Fig. 3.

[33] As they stand, Eqs. 10 and 11 have R and ε as independent parameters. Models where the capture range depends on the turbulence level are discussed further below. Given the form of the analytical results, we note that such a modification is easy to implement (Pécseli et al. 2012). For visual predators with an interception range R that is given for the actual species and local conditions (Aksnes and Giske 1993; Aksnes and Utne 1997; Urtizberea and Fiksen 2013), Eq. 7 presents a closed expression that is applicable when the turbulence conditions are known.

[34] As in other studies (Rothschild and Osborn 1988; MacKenzie et al. 1994; Osborn 1996) our analysis so far assumes that the volume and range of interception are independent of the intensity of the turbulence. The range R and the specific energy dissipation ε are then independent parameters for the problem. It is possible to extend the analysis to include the case where the capture range $R = R(\varepsilon)$ varies with the intensity of the turbulence. The number of independent parameters is then reduced by one. If $R = R(\varepsilon)$ is known, the generalization is simple and obtained by insertion in expressions such as Eqs. 10 and 11. We find, however, that the problem of turbulence-dependent range requires a more detailed analysis of the detection problem, as summarized in the next section.

Capture with Varying Turbulence Intensity

[35] The problem of prey or predator detection in a turbulent environment involves two issues: (1) the detection of disturbances induced by moving plankton and (2) the detection of disturbances caused by the turbulent flow variations. We distinguish detected signals originating from moving prey as v_{prey} and signals originating from the turbulent motions as v .

[36] Assume first that the flow around a predator is disturbed by prey moving in its vicinity, as illustrated

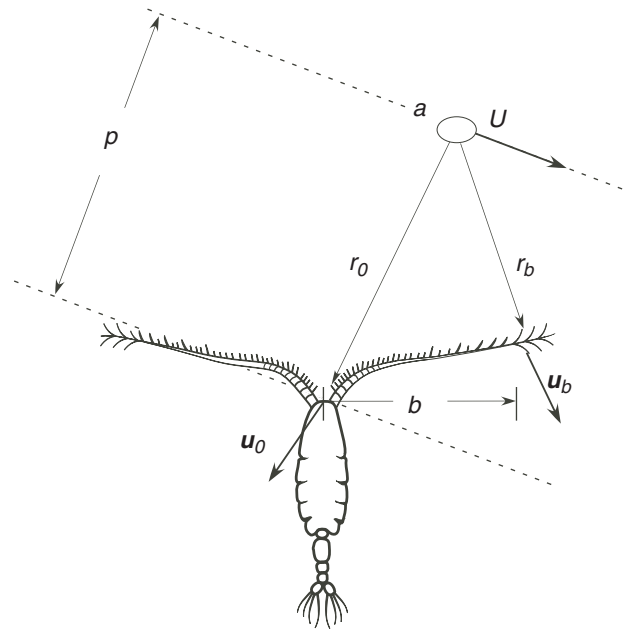


Fig. 4 Diagram for the velocity perturbation near a predator due to relative prey motions (after Visser 2001). The prey is indicated by its size a . It moves with a velocity U at an impact parameter p with respect to the predator, inducing velocity disturbances u_0 and u_b at the two ends of the predator's antennae with length b . For many cases we find that $b < \eta_0$, where η_0 is the Kolmogorov length. The flow dynamics on this scale should be described by expressions relevant for the viscous subrange.

in Fig. 4. The motions in the surrounding flow are perceived by the predator along its sensory organs (Jiang and Paffenhöfer 2008). Sensitivity seems here to be associated with velocity differences (rather than, e.g., acceleration) between the tip and the base of the antennae (Yen et al. 1992; Visser 2001; Kiørboe 2013). Little is known concerning details in the response of sensory organs of plankton to perturbations from different velocity components. When estimating probability densities for velocity differences in the following (see also Fig. 5B), we use the velocity difference $u_{\parallel 0} - u_{\parallel b}$ as representative for the dominant contribution to the velocity signal experienced by the copepod. The predator receives signal at all setae along the antennae, but with reference to the velocity structure function (the Kolmogorov–Obukhov law in the inertial range) it is argued that, on average, the largest velocity differences will be found at the largest separations, that is, the base and the tip of the antennae. The perpendicular component (as in Fig. 5A) will merely give rise to a local translation or rotation, and this is of little relevance here. We use the

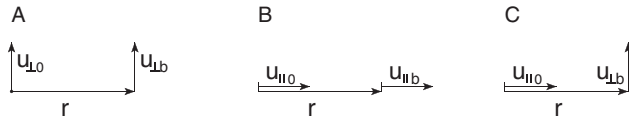


Fig. 5 Velocity components entering the construction of the velocity difference $v(t)$, where a case corresponding to A has one of the velocity vectors pointing out of the page (not shown).

velocity difference at the largest separation b (see Fig. 4), since smaller separations will, on average, give smaller differences. The signal defined here can take both signs, but little is known concerning the ability of plankton to distinguish the sign. For generality, we retain both signs rather than taking the absolute value.

[37] The prey-generated disturbance at the predator position diminishes with the separation between predator and prey (Kjørboe and Visser 1999; Kjørboe et al. 1999), but the velocity perturbation experienced in the surroundings of moving prey depends on a number of other parameters as well (Visser 2001): the distance r_0 between predator and prey, the impact parameter p (both defined in Fig. 4), the relative orientation, and so forth. For the present analysis the distance dependence of the strength of the perturbation is most important, so we focus on this. Depending on details in the prey propulsion (Visser 2001), we find that the strength of the velocity perturbation scales as AV_*/r^m , with distance r , for motion at low Reynolds numbers, where V_* is the prey velocity relative to the surrounding fluid. The exponent m characterizes the organism, while A is a dimensional parameter depending, for instance, on the size and shape of the organism; typically we have $m = 1, 2, 3$. With the given simple model, we estimate the detected velocity perturbation as

$$v_{\text{prey}}(t) \approx AV_* \left(\frac{1}{r_0^m(t)} - \frac{1}{r_b^m(t)} \right)$$

(see Fig. 4), where it is assumed that the predator is at rest with respect to the local fluid, at least during the time of interaction. An approximate expression for v_{prey} represents an average over all relative angles, where a numerical factor is included in the constant A . A characteristic time duration of the perturbation can be estimated as p/V_* , apart from a numerical constant

that depends on \sqrt{m} . The impact parameter p determines the closest distance between predator and prey with the given motion. For order-of-magnitude estimates we can use

$$v_{\text{max}} \sim \frac{mbAV_*}{p^{m+1}} \tag{12}$$

for the peak value of the velocity disturbance and

$$\tau_{\text{prey}} \sim \frac{p}{V_*} \tag{13}$$

for its time duration, where we implicitly assume that $r_{0,b} > b > a$ (see Fig. 4). The results for v_{max} and τ_{prey} will be compared with the magnitude and the duration of excursions in detected velocity signals that originate from the turbulent motions.

[38] Existing models for plankton moving in turbulent environments (Kjørboe and Saiz 1995; Saiz and Kjørboe 1995; Visser 2001) assume that prey moving with some velocity V_* is recognized by a predator if it generates a disturbance in the detected signal exceeding a certain threshold U_* with respect to the root-mean-square fluctuation level of the turbulence (although it is not clear how this level was defined). In a calm or nonturbulent environment, the threshold value of the velocity disturbance defines the reference detection range as the minimum distance needed for the perturbation to exceed the threshold level for a particular organism (Kjørboe and Saiz 1995; Kjørboe and Visser 1999). The actual value of the threshold U_* depends on the species considered, as well as other parameters, but in general we expect representative values in the range of $U_* \in \{0.01 - 0.1\} \text{ mm s}^{-1}$ for the velocity difference between base and tip of the antennae (Saiz and Kjørboe 1995; Visser 2001). In a turbulent environment the noise originating from the surrounding flow perturbations will mask disturbances originating from prey, so it is expected that only enhanced prey signals will allow detection. To generate larger-velocity perturbations, the predator-prey separations have to be reduced, as indicated also by Eq. 12. Basically, this assumption implies that the range of interception depends on the turbulence level, that is, that we have to use $R = R(\epsilon)$ in Eqs. 10 and 11 and not R and ϵ as independent parameters. A simple model was suggested

by Kiørboe and Saiz (1995) requiring $v_{\text{prey}} \geq U_* + \sigma$ for detection, where in our models $\sigma \approx \sqrt{C_K(\varepsilon b)^{1/3}}$ for capture ranges in the inertial subrange and $\sigma \approx b\sqrt{C_V\varepsilon/\nu}$ for b in the viscous subrange, with b defined in Fig. 4. Given a model for the prey-induced disturbance, this argument gives an expression of the form $R = R(\varepsilon)$, which can be directly incorporated in our models.

[39] The simple argument outlined here is, however, problematic in at least one respect: it implicitly assumes that the contribution to the signal originating from the turbulence is confined to a level $\pm\sigma$ as perceived by the predator, so that any excess signal is easily recognized, that is, that a large signal can unambiguously be associated with the presence of prey. This is not correct, not even for a Gaussian random signal, where we might find arbitrarily large signal excursions with varying probabilities. A representative model signal is shown in Fig. 6. To examine this problem in more detail, we obtain estimates of relevant probability densities from direct numerical solutions of the Navier–Stokes equation for turbulent conditions and analyze the frequency with which the velocity differences at the base and tip of the antennae exceeds some selected level. Also, an average of the time duration of such a velocity excess is relevant, and this is estimated as well.

Average Frequencies of Level Crossings

[40] A detailed description of signal excursions and their time duration due to turbulent velocity variations turns out to be somewhat complicated. For locally

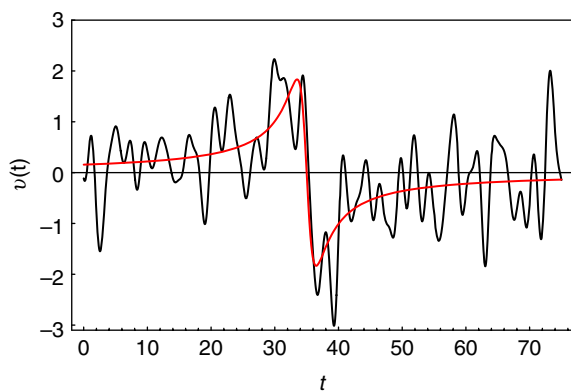


Fig. 6 Model of a signal $v(t)$ as a function of time t as induced by prey motions (red line), with additive random Gaussian noise (black line).

homogeneous isotropic turbulence we have analytical expressions (Davidson 2004) for the relations between second-order structure functions $\langle(u_{\perp 0} - u_{\perp b})^2\rangle$ and $\langle(u_{\parallel 0} - u_{\parallel b})^2\rangle$. The relevant statistical information is thus contained in the latter structure function. We will consequently consider only the parallel velocity components, writing $\langle v^2 \rangle = \langle(u_{\parallel 0} - u_{\parallel b})^2\rangle$.

[41] As it turns out, we will also need time derivatives of $v(t)$. These can be obtained from direct numerical solutions of particle trajectories in fully developed turbulence described by the Navier–Stokes equation. To obtain $dv(t)/dt$ we thus select two simulation particles representing the base and tip of an antenna at positions $\mathbf{r} = 0$ and $\mathbf{r} = \mathbf{b}$, with a particle separation b (see Fig. 4). The local volume element of the flow at the two positions has velocities $\mathbf{u}(\mathbf{r}, t)$ taken at $\mathbf{r} = 0$ and $\mathbf{r} = \mathbf{b}$, respectively. The time variability of the velocity signal, as detected by plankton in response to the variation of flow velocities, depends on unknown details in the interaction between the sensory organs and the local motions in the flow. Here we approximate $dv(t)/dt \approx \partial(\mathbf{u}(\mathbf{r}_0(t), t) - \mathbf{u}(\mathbf{r}_b(t), t)) \cdot \hat{\mathbf{b}}/\partial t$, obtained by following two particles passing $\mathbf{r} = 0$ and $\mathbf{r} = \mathbf{b}$ at time t , respectively. The scalar multiplication with the unit vector $\hat{\mathbf{b}}$ in the direction of \mathbf{b} ensures that the parallel velocity components are selected (see Fig. 5B). The relation between the partial derivative used here and the acceleration $\mathbf{u} \cdot \nabla \mathbf{u}$ entering the absolute derivative has been discussed elsewhere (Tsinober et al. 2001; Liberzon et al. 2012). To simplify the notation in the following, we write \dot{v} for the time derivative $dv(t)/dt$.

[42] The velocity difference $v(t)$, as well as $dv(t)/dt$, can take both positive and negative values, depending on the directions of the relevant velocity vectors. For locally homogeneous and isotropic turbulence, we have $\langle v(t) \rangle = 0$ and $d\langle v(t) \rangle/dt = 0$. The probability densities of $v(t)$ and $dv(t)/dt$ are slightly skewed due to intermittency effects. The signal $v_{\text{prey}}(t)$ induced by a passing prey can take both positive and negative values with the present definitions. It is likely that predators can distinguish the sign of these relative velocity perturbations (Kiørboe 2013), but we do not emphasize this in the present study.

[43] To obtain analytical expressions for the amplitudes discussed above, we analyze the problem in

terms of results from studies of noise in electronic circuits (Rice 1945; Bendat 1958). Note first that the time it takes for the signal $v(t)$ to cross a small interval dv is given as dv/\dot{v} . The fraction of time spent by the signal in an interval dt around a set of amplitudes and time derivatives $\{v, \dot{v}\}$ within a narrow interval $dvd\dot{v}$ is $P(v, \dot{v})dvd\dot{v}dt$ in terms of the joint probability density $P(v, \dot{v})$. The number of crossings of some signal level v within dt is then (Bendat 1958)

$$\frac{P(v, \dot{v})dvd\dot{v}dt}{dv/\dot{v}} = \dot{v}P(v, \dot{v})d\dot{v}dt. \tag{14}$$

[44] The average number $\langle \mathcal{N} \rangle$ of upward crossings of the level $v = U_*$ as a function of time duration t is then obtained by integration with respect to time (which becomes simple since $P(v, \dot{v})$ is independent of time), and then with respect to all positive values of \dot{v} . The result is

$$\langle \mathcal{N}(U_*) \rangle = t \int_0^\infty \dot{v}P(U_*, \dot{v})d\dot{v}, \tag{15}$$

directly proportional to time t .

[45] The average level crossing frequency $d\langle \mathcal{N}(U_*) \rangle/dt$ measures how often a signal exceeds the reference level U_* . By Eq. 15 we find this frequency to be constant. The fluctuating velocity difference over the antennae and the associated level crossings is interpreted as an error signal in the sense that it does not represent the presence of prey. The energy dissipation ϵ enters implicitly through $P(U_*, \dot{v})$, as demonstrated further below; in particular, it is not correct simply to assume the error signal to be proportional to ϵ .

[46] The analysis of the probability densities for time derivatives is related to acceleration statistics that has mostly been analyzed for absolute motion of single particles (Tsinober et al. 2001; Bec et al. 2006; Liberzon et al. 2012). The present problem concerns relative accelerations. Figs. 7 and 8 present results obtained by analyzing numerically obtained data from simulations of incompressible fluid turbulence. We have $P(v)$ with $v \equiv u_{||}(0, t) - u_{||}(r, t)$ in Fig. 7 for both the inertial and viscous subranges. Two universal scaling laws are obtained, where velocities are normalized by $\sqrt{r^2 \epsilon / \nu}$ in the viscous subrange and by $(r\epsilon)^{1/3}$ in the inertial subrange. The results are obtained for normalized separations $r/\eta_0 =$

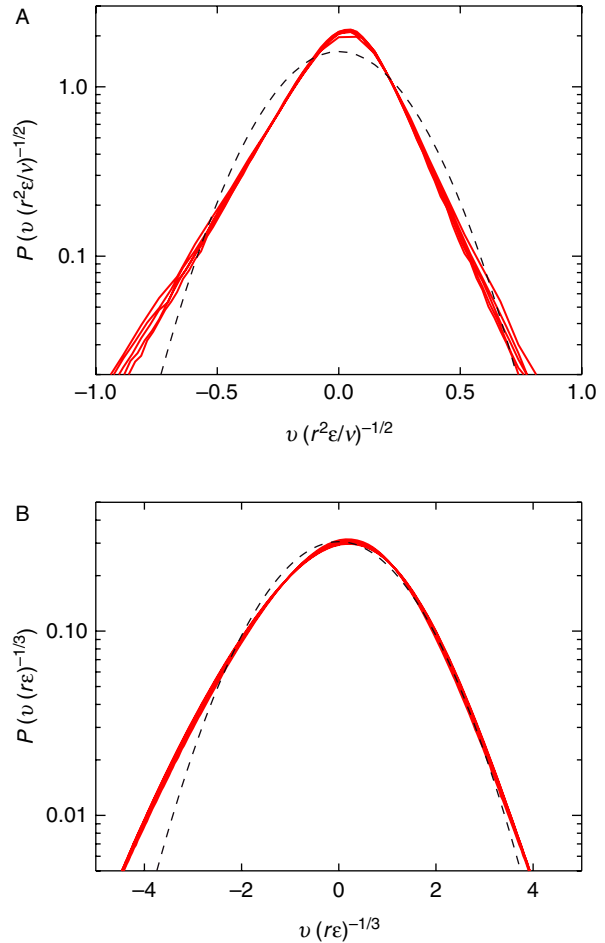


Fig. 7 Normalized probability densities for the longitudinal velocity differences $v(t)$ (see Fig. 5B) for the viscous and inertial subranges of turbulence. Spatial separations are in computational units 0.01, 0.015, 0.02, 0.025, and 0.03 for the viscous subrange in A and 0.25, 0.30, 0.35, 0.40, 0.45, and 0.50 for the inertial subrange in B. For comparison, we have the length scale $\eta_0 \approx 0.07$ in computational units to separate the viscous and inertial subranges. In the variables on axes we insert $r = b$ for the predator in Fig. 4. We have the specific energy dissipation $\epsilon = 0.810878$ as determined by the numerical energy input, while the kinematic viscosity used (for water) is $\nu = 8.8 \times 10^{-4}$ in computational units. The horizontal velocity axis in A is normalized by the root-mean-square velocity $(r^2 \epsilon / \nu)^{1/2}$ obtained for the viscous subrange at separations $r < \eta_0$. For the inertial subrange in B we normalize by $(r\epsilon)^{1/3}$, where $r > \eta_0$. Dashed lines give the best Gaussian fit in both cases. The skewness of the probability densities is an indicator for intermittency effects (Castaing et al. 1990).

0.143, 0.214, 0.285, 0.356, 0.428 for the viscous sub-range and $r/\eta_0 = 3.56, 4.27, 4.99, 5.70, 6.41, 7.12$ for the inertial subrange. The two subranges have significantly different universal scalings, the inertial scaling being independent of viscosity ν . Intermittency effects give rise to a skewness of the probability density in the

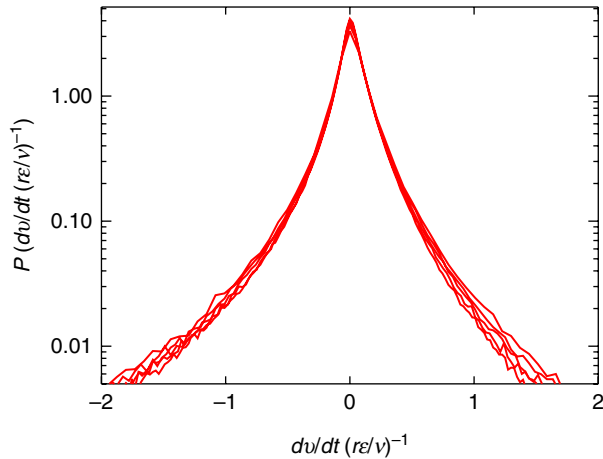


Fig. 8 Normalized probability densities for the time derivative $dv(t)/dt$ of the longitudinal velocity differences (see Fig. 5B) for the viscous range of the turbulence. Selected spatial separations r are in computational units 0.01, 0.015, 0.02, 0.025, and 0.03. We use the specific energy dissipation $\varepsilon = 0.810878$ as determined by the energy input in the numerical simulations. The kinematic viscosity is $\nu = 8.8 \times 10^{-4}$ in computational units. The velocity derivative is normalized by $(r\varepsilon/\nu)$ as relevant for the viscous subrange. Analysis of another data set (Péceli and Trulsen 2007) with different parameters ε and ν gives essentially identical results.

inertial limit. We find interesting indications of this skewness remaining also in the viscous limit, although not as pronounced as for the inertial range (Tennekes 1968, 1973).

[47] As an example we consider the smallest scales addressed above (see “Encounters: Brownian diffusion range”), where we have spatial separations of the order of 100 μm . According to Fig. 7A for the viscous subrange, we require $v \ll b/\tau_K$ to find large probabilities for velocity differences. The conditions for significant velocity variations over an organism on these small scales are then found by taking $b \approx 100 \mu\text{m}$. Parameters found in the coastal zones (see Table 1) give $\tau_K \sim 0.1 - 3.0 \text{ s}$, implying that $v \ll 0.3 - 1.0 \text{ mm s}^{-1}$ for these smallest Brownian scales. According to Fig. 7 there is a significant probability of finding velocities in a range around $v \sim 0.1 \text{ mm s}^{-1}$ for these conditions. Although small, these velocity differences can still contribute to turbulent transport. The arguments ignored motions produced by the organisms themselves. Even small motions of the appendices of organisms on the 10- to 100- μm scales can induce velocities larger than those caused by turbulent motions on these same scales. Previously, we found that thermal motions can also become important for

these smallest scales when the turbulence level is small, as in the open ocean (see Table 1).

[48] Fig. 8 shows the probability density for the normalized $P(\dot{v})$, here only for the viscous subrange. A universal scaling law with a velocity derivative normalization $r\varepsilon/\nu$ is fulfilled. The analysis has been extended to include a different numerical simulation where the numerical dissipation rate was $\varepsilon = 0.8853$ and where the numerical viscosity was changed from $\nu = 8.8 \times 10^{-4}$ to $\nu = 2.05 \times 10^{-3}$, giving the same excellent agreement with the proposed scaling (with ε and ν in numerical dimensionless units). It is interesting to note that $P(\dot{v})$ can be well approximated by a so-called κ -distribution. Such distributions seem to result from random increments governed by Levy flight probability distributions (Collier 1993).

[49] While we find that a Gaussian model might be useful as an approximation for $P(v)$ (see Fig. 7), it fails completely for $P(\dot{v})$. Figs. 7 and 8 show the marginal probability densities $P(v)$ and $P(\dot{v})$ in normalized form. Fig. 9 shows the full joint probability density $P(v, \dot{v})$

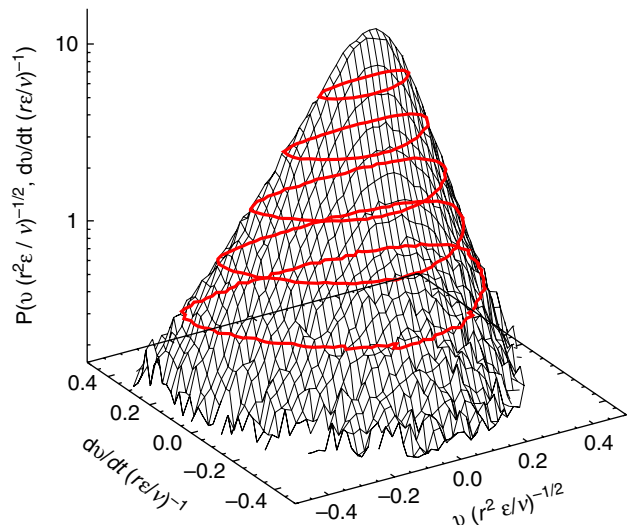


Fig. 9 Normalized joint probability density $P(v\sqrt{r^2\varepsilon/\nu}, \dot{v}(r\varepsilon/\nu))$ for the normalized longitudinal velocity differences $v(t) \equiv u_{||0}(t) - u_{||b}(t)$ (see Fig. 5B) and their time derivative $dv(t)/dt \equiv \dot{v}$, for separations r in the viscous subrange of turbulence. We have the specific energy dissipation $\varepsilon = 0.810878$ in the numerical simulations, whereas the kinematic viscosity used is $\nu = 8.8 \times 10^{-4}$ in computational units. The projections of the probability densities for v and $dv/dt \equiv \dot{v}$ are those shown in Figs. 7 and 8. Velocities and velocity derivatives are normalized as appropriate for the viscous subrange, just as in Figs. 7 and 8. Selected levels of constant probability are shown in red.

from which the marginal probability densities (or projections) given in Figs. 7 and 8 can be derived. The signals $v(t)$ and $\dot{v}(t)$ are uncorrelated since $\langle v(t)dv(t)/dt \rangle = \frac{1}{2}d\langle v^2(t) \rangle/dt = 0$ for time-stationary processes, but they are not independent; that is, $P(v, \dot{v}) \neq P(v)P(\dot{v})$. Using the results in Fig. 9, we find the average level crossing frequency $d\langle \mathcal{N}(U_*) \rangle/dt$ as shown in Fig. 10. The number of level crossings per time unit is expressed in terms of the Kolmogorov time $\tau_K \equiv \sqrt{\nu/\varepsilon}$. The number of level crossings is of the order 10 within a Kolmogorov time τ_K for $U_* \approx 0$. Recall here that we consider the viscous subrange where the variations are on length scales comparable to or shorter than η_0 .

[50] For illustration of these results, we consider a Gaussian reference case. This model has limited accuracy, but it retains the correct parameter scalings (Rollinson 1978; Pécseli et al. 2012) and can give the correct orders of magnitude, an advantage of the model being a closed and simple analytical form. Ignoring intermittency effects and taking ε to be a deterministic constant, we thus assume that the probability density for the

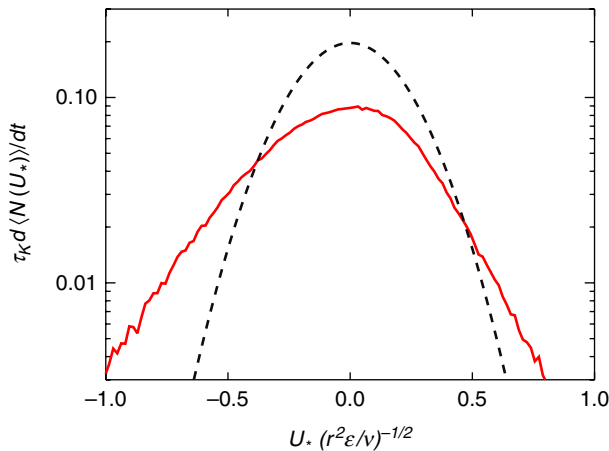


Fig. 10 Frequency $d\langle \mathcal{N}(U_*) \rangle/dt$ of the crossings with positive time derivative of a normalized level $U_*/(r^2\varepsilon/\nu)^{1/2}$ of the signal defined as $v(t) \equiv u_{||a}(t) - u_{||b}(t)$ for the turbulent velocity component differences. The frequency of such level crossings is measured in units of the inverse Kolmogorov time $\tau_K^{-1} \equiv \sqrt{\varepsilon/\nu}$. This frequency can be used to measure how frequently a predator perceives a large-velocity variation along its antennae. Large-amplitude excursions in the velocity (as determined by U_*) will have smaller frequencies, that is, occur rarely. The result is obtained by the integral in Eq. 15 and is shown by the red line for varying levels of U_* . We use $P(v, \dot{v})$ obtained from the numerical simulations (see Fig. 9). The dashed line gives the result from a Gaussian random process with the same standard deviations as for v and \dot{v} . (The dashed line is not obtained by fitting a Gaussian to the solid curve.)

signal $v(t)$ is

$$P(v) = \frac{1}{\sigma\sqrt{2\pi}} e^{-\frac{1}{2}v^2/\sigma^2}, \tag{16}$$

where $\sigma^2 = \langle v^2 \rangle = C_V b^2 \varepsilon/\nu$ in terms of the separation b defined in Fig. 4. For stationary processes, v and \dot{v} are uncorrelated. For this special Gaussian model, the signal v and its time derivative \dot{v} are also statistically independent (since they are uncorrelated Gaussian processes), so that $P(v, \dot{v}) = P(v)P(\dot{v})$. Thus,

$$\frac{d\langle \mathcal{N}(U_*) \rangle}{dt} = \frac{1}{2\pi} \frac{\sigma'}{\sigma} e^{-\frac{1}{2}U_*^2/\sigma'^2}, \tag{17}$$

where $\sigma' = \sqrt{\langle \dot{v}^2 \rangle}$ is the standard deviation for \dot{v} . By dimensional arguments we can estimate the ratio σ'/σ . Dimensionally we have the ratio σ/σ' to be a characteristic time scale. For the viscous subrange we have $\sigma'/\sigma \approx \sqrt{\varepsilon/\nu}$. This ratio is independent of b , but if large antennae with $b > \eta_0$ were considered, a b -dependence would appear. The dependence on b is found in the exponent of Eq. 17.

[51] Eq. 17 can be used to measure the time variability of the velocity signal obtained by the antennae of plankton. In this case we have a good measure in the number of upward zero crossings per time unit for $U_* = 0$,

$$\frac{d\langle \mathcal{N}(U_* = 0) \rangle}{dt} \approx \frac{1}{2\pi} \sqrt{\frac{\varepsilon}{\nu}}, \tag{18}$$

for $b < \eta_0$. The factor $1/2\pi$ has a basis in the analysis, but other numerical coefficients in Eq. 18 are uncertain and therefore omitted. Small b makes the antennae less sensitive to turbulent noise, but at the same time also less sensitive to velocity variations induced by moving prey, because for small spatial separations the velocity differences are also small.

[52] The reference Gaussian case is given by a dashed line in Fig. 10. We find that this nonintermittent limit has limited applicability for the present problem, but it contains the correct scaling with parameters b , ε , and ν and can serve as an order-of-magnitude estimate. While the Gaussian approximation gives a level crossing frequency that falls off as $e^{-U_*\tau_K/r}$ for large U_* , we find that the results in Fig. 10 are best described by a level crossing frequency scaling as $e^{-|U_*\tau_K/r|}$ for large

$U_*\tau_K/r$. For values of $|U_*| > 0.5b/\tau_K$, the Gaussian result thus gives level crossing frequencies that are too small.

Average Duration of Level Crossings

[53] The analysis outlined so far has addressed the problem of the frequency of excess signals detected by organisms perceiving velocity differences. Such signals compete with signals indicating the presence of prey. However, the argument addressed only the frequency of excursions in the signal. To complete the argument we also need an indicator of the duration of excesses: if these are significantly different for prey and noise, then it is possible for the predator to avoid confusion. For the duration of the prey-induced velocity perturbation we have, apart from a numerical factor, $\tau_{\text{prey}} \sim p/V_*$ for a given prey velocity V_* with respect to the local flow at an impact parameter p (see Fig. 4). The impact parameter that gives rise to a selected peak value U_* of the velocity difference perturbation $v_{\text{prey}}(t)$ was found by Eq. 12 to be $p_* \approx (mbAV_*/U_*)^{1/(m+1)}$, giving a corresponding time duration $\tau_{\text{prey}} \sim (mbAV_*/U_*)^{1/(m+1)}/V_* = (mbA/U_*)^{1/(m+1)}/V_*^{m/(m+1)}$. Compared with slower prey, rapidly moving prey with the same impact parameter p induces a relative velocity disturbance with a shorter duration as observed by the predator. By these foregoing expressions we have relations that express the peak value of the detected velocity signal v_{max} and the time duration of the detected signal by Eq. 13, all expressed in terms of the prey velocity V_* and the selected velocity difference threshold level U_* .

[54] For random noise we can generally argue (see Kristensen et al. 1991) that an average time $\langle T \rangle$ between an upward and a downward crossing of a level U_* is estimated (although not an exact analytical result) by the average time spent above a reference level divided by the number of upward crossings; that is,

$$\langle T(U_*) \rangle = \frac{\int_{U_*}^{\infty} P(v)dv}{\int_0^{\infty} \dot{v}P(U_*, \dot{v})d\dot{v}}. \quad (19)$$

The result obtained for the present problem is shown in Fig. 11. We find by inspection of the figure that the average duration of positive excursions of the velocity

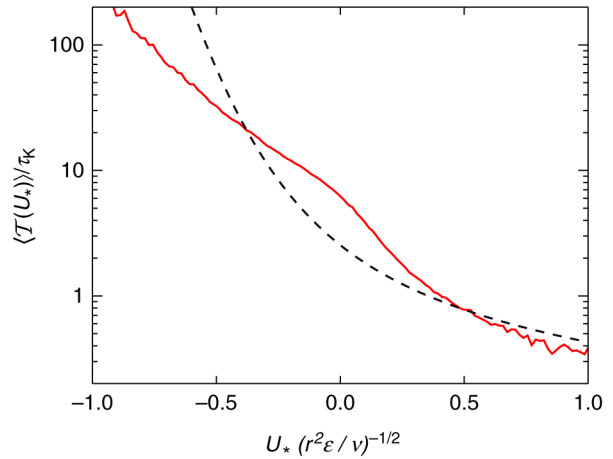


Fig. 11 Average duration $\langle T \rangle$ of the time intervals spent above a selected signal level U_* (red line). This result, obtained by Eq. 19, can be used to measure the average duration of pulsations in the velocity variations along the predator’s antennae, where different amplitudes in the velocity variations (given by U_*) will have different durations. The time durations are given in units of the Kolmogorov time τ_K (see Table 1). Taking a large negative value of the threshold level U_* , we find that almost all of the signal is above this reference level, and $\langle T \rangle / \tau_K$ diverges as $U_* \rightarrow -\infty$. A dashed line gives the reference Gaussian result.

difference $v(t)$ between base and tip of the antennae of a copepod is $7\tau_K$ or less. For large negative U_* , all of the time is spent above the reference level, so $\langle T(U_*) \rangle$ is diverging for $U_* \rightarrow -\infty$.

[55] The presentation in Fig. 11 concerns only the case of the average duration from an upward crossing of a reference level to the first downward crossing of the same level. The analysis of the average time duration from a downward crossing to the first upward crossing of the same level can be analyzed by precisely the same arguments as used above. The results are not strictly symmetric to those in Fig. 11 because of intermittency effects that imply a slight skewness of the relative velocity signal. We can, however, still use Fig. 11 as illustrative by letting only the part with $U_* r \sqrt{\epsilon/\nu} \geq 0$ represent $|U_*|$.

[56] Again, we can give the result that would be obtained from a Gaussian random process (Kristensen et al. 1991),

$$\langle T(U_*) \rangle = \pi \frac{\sigma}{\sigma'} e^{1/2 U_*^2 / \sigma^2} \times \text{erfc} \left(\frac{1}{\sqrt{2}} U_* / \sigma \right), \quad (20)$$

where $\text{erfc}(x) \equiv (2/\sqrt{\pi}) \int_x^{\infty} e^{-\xi^2} d\xi$ is the complementary

error function. For large U_* the Gaussian limit has the simple result $\langle \mathcal{T}(U_* \rightarrow \infty) \rangle = \sqrt{2\pi}(\sigma^2/\sigma')/U_*$. Inspection of Fig. 11 indicates that for large U_* the $1/U_*$ variation of the Gaussian model is in acceptable agreement with the results, albeit with a modified numerical coefficient. Note that the statistical uncertainties due to the finite data set when estimating $P(v, \dot{v})$ become noticeable for large U_* in Fig. 11.

Discussion

[57] We have summarized analytical results for planktonic predator–prey encounter and capture rates. Some of the results are known from the literature (Rothschild and Osborn 1988; Osborn 1996; Mann et al. 2005) and, in particular, also from numerical simulations (Pécseľi and Trulsen 2007; Pécseľi et al. 2012) but are here presented in a simplified version amenable for comparison with observations. The range of validity of the results is generalized to the smallest scales (identified as the Batchelor scale), where Brownian motions also become of importance, and we argued that this limit can be relevant for organisms on 100- μm scales. The analysis is formulated in terms of as few parameters as possible. The flow (i.e., water) is characterized by its kinematic viscosity ν , turbulence by the specific dissipation rate ε , and plankton by its encounter or capture range R , an opening angle θ of its field of perception, and a time $\Delta\tau$ needed for capturing prey. With this information, and possibly added characteristic velocities for predator and prey, we can predict encounter rates and capture probabilities in terms of some constants and an empirically obtained universal probability density for transit times. Results are presented in terms of statistical averages and do not directly apply to individual observations. We find a characteristic dome-shaped average capture rate (MacKenzie et al. 1994), as illustrated in Fig. 3, with an optimum turbulence level given as $\varepsilon \approx 0.35R^2/\Delta\tau^3$. The results agree with observations in nature (MacKenzie and Kiørboe 2000). Considering individual species and different capture processes, other parameters may also be of importance (relative orientations of predator and prey, etc.), but the parameters selected here are universal and relevant for all plankton.

[58] The capture range, or range of interception R , can depend on many local parameters, such as light

conditions (Fiksen et al. 1998). The basic results from our previous studies apply as long as R can be considered constant, that is, when these local conditions are unchanged. For visual predators (Aksnes and Giske 1993; Aksnes and Utne 1997) we can argue that this assumption of a fixed value for R is justified. Ideas for letting the interception distance R vary with the turbulence level have been suggested: basically, in a turbulent environment prey has to be closer to a predator for its motions to be detected compared with quiet conditions (Saiz and Kiørboe 1995). Such modifications are readily included in our models by letting $R = R(\varepsilon)$, rather than having R and ε be independent variables. Such a model relies on the assumption that disturbance from prey can be unambiguously distinguished from turbulent fluctuation. We argued, however, that a clear distinction of the origin of perturbations detected by the antennae of a copepod is not logically possible. To have a simple yet realistic model for a comparison of prey-induced signals and turbulent noise, we introduce two simple models (Eqs. 12 and 13) for the strength and duration of a signal generated by prey in the vicinity of a predator. Typical perturbations induced by moving prey scale as $mbAV_*/p^{m+1}$ in terms of prey velocity V_* and impact parameter p (see Fig. 4), with $m = 1, 2, 3$ for relevant cases (Visser 2001). Rapidly moving prey can be recognized as giving a large-amplitude signal. There may be good reasons for prey to move rapidly, because this reduces the time available for capture and thus the capture probability, but this advantage is thus not without drawbacks. Slowly moving prey induce velocity variations in the flow around the predator with slowly varying disturbances (with a duration $\sim b/V_*$) that can be mistaken for turbulence-induced perturbations, whereas rapid motion gives a signal that can be distinguished from the turbulence.

[59] To quantify the probabilities of observing a certain amplitude level of turbulence-induced signals, we use the average frequency for the velocity difference between base and tip of a copepod's antennae to cross a selected threshold level, say, U_* . Analytical expressions for this frequency require the joint probability density $P(v, \dot{v})$ of the signal $v(t)$ and its time derivative $\dot{v}(t)$ to be known. We obtain $P(v, \dot{v})$ by analyzing numerical solutions of the Navier-Stokes equation obtained for

turbulent conditions. The result is shown in Fig. 8, and the average frequency for $v(t)$ to exceed some threshold level U_* is shown in Fig. 10. We normalized U_* with $r\sqrt{\varepsilon/\nu} \equiv r/\tau_K$, where for R we insert the relevant value for b . Times are measured in units of the Kolmogorov time τ_K . We inserted a dashed line in Fig. 10 for the Gaussian reference case. Although this Gaussian model retains the correct dimensionless scaled variables, we find that it serves best as a guide for orders of magnitude only. In the coastal zones used for reference above, we have $\tau_K \sim 0.1 - 3.0$ s. Taking, for instance, $\tau_K = 3$ s, the results in Fig. 10 imply that the velocity difference between base and tip of a 3-mm antenna of a copepod exceeds 0.5 mm s^{-1} on average every 150 s. We can consider one more example by noting that studies of *Labidocera* (Yen et al. 1992) demonstrated that their large spike receptor may be considered a relative velocity detector, requiring only a $20 \text{ } \mu\text{m s}^{-1}$ velocity difference of fluid across the antenna to trigger a neural response. For this case we will have $U_*b/\tau_K \ll 1$ for most realistic parameters. This velocity level will correspond to values near the origin of the abscissa in Fig. 10 and will be exceeded due to turbulent motions on average once in ~ 10 Kolmogorov times τ_K , that is, on average every 30 s for the coastal zone conditions mentioned above. Related studies (Yen et al. 1992; Svensen and Kiørboe 2000; Kiørboe 2013) indicate that velocities less than $100 \text{ } \mu\text{m s}^{-1}$ can elicit attack, although these values depend on orientation, light conditions, and so on. Again, we can use Fig. 10 to estimate the frequency of occurrence of velocity differences $v \sim 100 \text{ } \mu\text{m s}^{-1}$ and find, again using $b = 3 \text{ mm}$ and $\tau_K = 3 \text{ s}$, that this level is exceeded on average once every 35 s.

[60] We also argued that the time duration of the velocity perturbation can serve to distinguish prey from turbulence-induced noise. If the time scale for the velocity variations due to turbulence are long compared with the duration of the passage of prey, we expect the prey signal with duration $\tau_{\text{prey}} \sim p/V_*$ to appear as a localized or narrow “spike” that is readily recognizable, even if the long time variations of the turbulent signal can have a large amplitude. This effect will be most conspicuous in the open ocean, where small values of ε imply variations with a long time scale of $v(t)$ (see Table 1). In the other extreme, where the turbulent

motions are very rapid, for instance, at the tidal front with large ε (see Table 1), a comparatively slow velocity perturbation due to prey motion can modulate the turbulence signal (see Fig. 6), and if the amplitude in this modulation is sufficiently strong, it can again be recognizable. Fig. 6 illustrates such a case. For this latter scenario to become effective, within the time duration τ_{prey} (given in Eq. 13) of the perturbation induced by the predator there should be a negligible probability for the turbulent relative velocity fluctuations $v \equiv u_{\parallel}(0, t) - u_{\parallel}(b, t)$ to exceed the perturbations induced by the prey, whose velocity amplitude is $v_{\text{max}} \sim mbAV_*/p^{m+1}$. We can take this problem as a case for illustrating the use of Figs. 10 and 11. Measuring τ_{prey} in units of τ_K , we can use Fig. 11 to estimate the normalized magnitude $U_*/\sqrt{b^2\varepsilon/\nu} = U_*\tau_K/b$ of the perturbation that gives rise to a velocity excursion of that selected duration. Having obtained a characteristic turbulent velocity this way, we can then use Fig. 10 to estimate how often it occurs within a Kolmogorov time τ_K . As a numerical example, we take conditions for the shelf or the coastal zone (see Table 1), with $\tau_K = 3$ s, and consider a predator with antennae where $b = 5 \text{ mm}$, which is amply within the viscous subrange here. Depending on the other relevant predator characteristics, these parameters can be close to those giving the optimum conditions in Fig. 3. Given an impact parameter of, say, $p = 5 \text{ mm}$ and a velocity $V_* = 2 \text{ mm s}^{-1}$, the duration of the velocity perturbation induced by moving prey is of the order of $1 - 2 \tau_K$. Turbulence-created perturbations with a similar duration have $U_*\tau_K/b \approx 0.25$ according to Fig. 11. Using Fig. 10, we find that this happens on average once every 10–15 τ_K . With a prey concentration of, for instance, 50 L^{-1} , then according to Eq. 2 the turbulence will give an encounter rate of 0.1 s^{-1} , corresponding here to once every 5–10 τ_K on average. This value refers to a predator moving passively with the flow. For predators with self-induced motions, the encounter rate will be larger (see Eq. 7). For the selected parameters, the predator will receive more “true” signals from prey than “false” signals from the turbulent motions. For this case we can thus use a fixed value for the range of interception R , and the results summarized in the “Results” section apply. Figs. 10 and 11 serve as tools for describing how a copepod perceives a turbulent

environment. The figures are based on a few essential parameters only but are easy to apply in practice.

[61] The arguments concerning the turbulence-induced false signals can be applied for prey as well: turbulent motions can incorrectly be interpreted as evidence for a nearby predator. It is thus interesting that there are observations of the copepod *Acartia clausi* increasing the number of escape reflexes, apparently directly in response to enhanced turbulence levels (Saiz and Alcaraz 1992b). MacKenzie and Kiørboe (1995) observed the feeding and swimming behavior of freely swimming cod (*Gadus morhua*) and herring (*Clupea harengus*) larvae in calm and turbulent ($\varepsilon \sim 7.4 \times 10^{-8} \text{ mm}^2 \text{ s}^{-3}$) laboratory environments at limiting and satiating abundances of *Acartia tonsa*. They observed that attack position rates were significantly higher in turbulent than in calm water at low food abundances for the two size groups of cod. The difference in cod attack position rate between calm and turbulent water was much less when prey were more abundant. Attack position rates of herring larvae were higher in turbulent water than in calm water; however, the difference was less significant.

[62] The discussion of the encounter rate J_∞ in the present study referred to predator-prey encounters but will apply equally well to a related analysis of mating of plankton by estimating an average number of male-female encounters per time unit.

Significance to Aquatic Environments

[63] Turbulence presents the most effective mixing mechanism available in nature. It affects flow motions on a variety of scales, from global circulation patterns down to the Batchelor scale, where classical thermal diffusion begins to have a role. Turbulence will, in particular, have a role in the feeding rate of plankton. The analytical expressions describing these effects take different forms depending on the scale sizes they describe. The present work concentrates on the viscous and the inertial subranges for conditions where locally homogeneous and isotropic turbulence can be assumed. The results are presented in terms of statistical averages. Information about the motion of individual organisms is thus lost. Analytical approximations are given as functions of scaled variables expressed in terms of basic

parameters of the problem. The water is characterized by its kinematic viscosity ν , and turbulence, by the specific energy dissipation ε . The volume where plankton observes and captures prey is modeled as conical form with radius R and an opening angle θ , where hemispheres with $\theta = 90^\circ$ and spheres with $\theta = 180^\circ$ are special cases. Motion of plankton is characterized by a velocity and a time $\Delta\tau$ needed for capturing prey. It is an advantage to use dimensionless scaled variables so that compact expressions can be obtained in terms of, for instance, $R^3\sqrt{\varepsilon/\nu}$, as in Eq. 3, instead of using R , ε , and ν individually, thus greatly simplifying experimental or numerical testing of the expressions.

[64] While turbulence enhances encounter rates, it can also have adverse effects for a predator by reducing capture rates. We argued that there can be two different reasons for this: reducing the time available for capture, and generating noise in the signals detected by the antennae of predators. Describing the latter problem, we need the joint probability density of velocity difference across the predator's antennae, as well as the time derivative of this signal. These probability densities were obtained empirically by using data from numerical simulations. The present analysis provides tools for estimating the frequency of occurrence of the magnitude of the fluctuations in velocity differences over antenna lengths and allows estimates of the average durations of such velocity perturbations. For low turbulence levels, the velocity variations $v(t)$ have long time scales and small amplitudes; thus, the turbulence contributes to the predator-prey encounter rate without causing disturbing noise.

[65] Several of the results summarized in the first part of the present work have already been tested by observations of plankton, by laboratory experiments, or by numerical simulations. The results that follow have the advantage of clearly separating turbulent sub-ranges. The results presented for Brownian diffusion range address the smallest scales where thermal motions compete with turbulent motions. The importance of this range has been speculated but not studied in greater detail. Current numerical simulations will be of little use here, since they (usually) do not include thermal motions. Calculations of plankton response to turbulent motions in the surroundings are open for direct

laboratory tests: plankton can be exposed to a turbulent environment in a laboratory where the specific energy dissipation ε can be controlled. It is then possible to directly observe the frequency of escape or attack reactions that are induced solely by turbulent motions.

Acknowledgments We thank G. Boffetta, J. Mann, S. Ott, J. E. Stiansen, and S. Sundby for valuable discussions. The database used for the numerical simulations can freely be downloaded from cfd.cineca.it/. Conditions for usage are given at cfd.cineca.it/cfd/repository/folder.2006-01-20.4761556357/document.2006-01-20.5299514280/. The supercomputing center Cineca (Bologna, Italy) is acknowledged for hosting the data.

References

- Aksnes, D. L., and J. Giske. 1993. A theoretical model of aquatic visual feeding. *Ecol. Modell.* **67**: 233–250. doi:10.1016/0304-3800(93)90007-F.
- Aksnes, D. L., and A. C. W. Utne. 1997. A revised model of visual range in fish. *Sarsia* **82**: 137–147. doi:10.1080/00364827.1997.10413647.
- Barange, M., J. G. Field, R. P. Harris, E. E. Hofmann, R. I. Perry, and F. E. Werner [eds.]. 2010. *Marine Ecosystems and Global Change*. Oxford University Press. doi:10.1093/acprof:oso/9780199558025.001.0001
- Barton, A. D., B. A. Ward, and M. J. Follows. 2013. The impact of organism-scale fluid turbulence on phytoplankton nutrient uptake rates and community structure. Pp. 5–6. *In* Abstracts from “Microscale Interactions in Aquatic Environments,” École de Physique des Houches, 10th–15th March 2013.
- Batchelor, G. K. 1959. Small-scale variation of convected quantities like temperature in turbulent fluid. Part 1. General discussion and the case of small conductivity. *J. Fluid Mech.* **5**: 113–133. doi:10.1017/S002211205900009X.
- Bec, J., L. Biferale, G. Boffetta, A. Celani, M. Cencini, A. Lanotte, S. Musacchio, and F. Toschi. 2006. Acceleration statistics of heavy particles in turbulence. *J. Fluid Mech.* **550**: 349–358. doi:10.1017/S002211200500844X.
- Bendat, J. S. 1958. *Principles and Applications of Random Noise Theory*. Wiley.
- Biferale, L., G. Boffetta, A. Celani, B. Devenish, A. Lanotte, and F. Toschi. 2004. Multifractal statistics of Lagrangian velocity and acceleration in turbulence. *Phys. Rev. Lett.* **93**, 064502. doi:10.1103/PhysRevLett.93.064502.
- Biferale, L., G. Boffetta, A. Celani, A. Lanotte, and F. Toschi. 2005. Particle trapping in three-dimensional fully developed turbulence. *Phys. Fluids* **17**, 021701. doi:10.1063/1.1846771.
- Biferale, L., G. Boffetta, A. Celani, A. Lanotte, and F. Toschi. 2006. Lagrangian statistics in fully developed turbulence. *J. Turbul.* **7**, N6. doi:10.1080/14685240500460832.
- Buckingham, E. 1914. On physically similar systems; illustrations of the use of dimensional equations. *Phys. Rev.* **4**: 345–376. doi:10.1103/PhysRev.4.345.
- Caparroy, P., U. H. Thygesen, and A. W. Visser. 2000. Modelling the attack success of planktonic predators: Patterns and mechanisms of prey size selectivity. *J. Plankton Res.* **22**: 1871–1900. doi:10.1093/plankt/22.10.1871.
- Castaing, B., Y. Gagne, and E. J. Hopfinger. 1990. Velocity probability density functions of high Reynolds number turbulence. *Physica D* **46**: 177–200. doi:10.1016/0167-2789(90)90035-N.
- Chandrasekhar, S. 1954. Stochastic problems in physics and astronomy. Pp. 3–91. *In* N. Wax [ed.], *Selected Papers on Noise and Stochastic Processes*. Dover.
- Collier, M. R. 1993. On generating kappa-like distribution functions using velocity space Lévy-flights. *Geophys. Res. Lett.* **20**: 1531–1534. doi:10.1029/93GL01702.
- Davidson, P. A. 2004. *Turbulence: An Introduction for Scientists and Engineers*. Oxford University Press.
- Evans, G. T. 1989. The encounter speed of moving predator and prey. *J. Plankton Res.* **11**: 415–417. doi:10.1093/plankt/11.2.415.
- Fiksen, Ø., A. C. W. Utne, D. L. Aksnes, K. Eiane, J. V. Helvik, and S. Sundby. 1998. Modelling the influence of light, turbulence and ontogeny on ingestion rates in larval cod and herring. *Fish. Oceanogr.* **7**: 355–363. doi:10.1046/j.1365-2419.1998.00068.x.
- Granata, T. C., and T. D. Dickey. 1991. The fluid mechanics of copepod feeding in turbulent flow: A theoretical approach. *Prog. Oceanogr.* **26**: 243–261. doi:10.1016/0079-6611(91)90003-5.
- Heath, M. R., E. W. Henderson, and D. L. Baird. 1988. Vertical-distribution of herring larvae in relation to physical mixing and illumination. *Mar. Ecol. Prog. Ser.* **47**: 211–228. doi:10.3354/meps047211.
- Incze, L. S., D. Hebert, N. Wolff, N. Oakey, and D. Dye. 2001. Changes in copepod distributions associated with increased turbulence from wind stress. *Mar. Ecol. Prog. Ser.* **213**: 229–240. doi:10.3354/meps213229.
- Jiang, H., and G. A. Paffenhöfer. 2008. Hydrodynamic signal perception by the copepod *Oithona plumifera*. *Mar. Ecol. Prog. Ser.* **373**: 37–52. doi:10.3354/meps07749.
- Jumars, P. A., J. H. Trowbridge, E. Boss, and L. Karp-Boss. 2009. Turbulence-plankton interactions: A new cartoon. *Mar. Ecol.* **30**: 133–150. doi:10.1111/j.1439-0485.2009.00288.x.
- Karp-Boss, L., E. Boss, and P. A. Jumars. 1996. Nutrient fluxes to planktonic osmotrophs in the presence of fluid motion. *Oceanogr. Mar. Biol.* **34**: 71–107.
- Kjørboe, T. 2008. *A Mechanistic Approach to Plankton Ecology*. Princeton Univ. Press.
- Kjørboe, T. 2011. How zooplankton feed: Mechanisms, traits and trade-offs. *Biol. Rev. Camb. Philos. Soc.* **86**: 311–339. doi:10.1111/j.1469-185X.2010.00148.x.

- Kjørboe, T. 2013. Attack or attacked: The sensory and fluid mechanical constraints of copepods predator-prey interactions. *Integr. Comp. Biol.* **53**: 821–831. doi:10.1093/icb/ict021.
- Kjørboe, T., H. Jiang, and S. P. Colin. 2010. Danger of zooplankton feeding: The fluid signal generated by ambush-feeding copepods. *Proc. Biol. Sci.* **277**: 3229–3237. doi:10.1098/rspb.2010.0629.
- Kjørboe, T., and B. R. MacKenzie. 1995. Turbulence-enhanced prey encounter rates in larval fish: Effect of spatial scale, larval behaviour and size. *J. Plankton Res.* **17**: 2319–2331. doi:10.1093/plankt/17.12.2319.
- Kjørboe, T., and E. Saiz. 1995. Planktivorous feeding in calm and turbulent environments, with emphasis on copepods. *Mar. Ecol. Prog. Ser.* **122**: 135–145. doi:10.3354/meps122135.
- Kjørboe, T., E. Saiz, and A. W. Visser. 1999. Hydrodynamic signal perception in the copepod *Acartia tonsa*. *Mar. Ecol. Prog. Ser.* **179**: 97–111. doi:10.3354/meps179097.
- Kjørboe, T., and A. W. Visser. 1999. Predator and prey perception in copepods due to hydromechanical signals. *Mar. Ecol. Prog. Ser.* **179**: 81–95. doi:10.3354/meps179081.
- Kristensen, L., M. Casanova, M. S. Courtney, and I. Troen. 1991. In search of a gust definition. *Boundary-Layer Meteorol.* **55**: 91–107. doi:10.1007/BF00119328.
- Lewis, D. M. 2003. Planktonic encounter rates in homogeneous isotropic turbulence: The case of predators with limited fields of sensory perception. *J. Theor. Biol.* **222**: 73–97. doi:10.1016/S0022-5193(03)00015-8.
- Lewis, D. M., and S. I. Bala. 2006. Plankton predation rates in turbulence: A study of the limitations imposed on a predator with a non-spherical field of sensory perception. *J. Theor. Biol.* **242**: 44–61. doi:10.1016/j.jtbi.2006.01.035.
- Lewis, D. M., and T. J. Pedley. 2001. The influence of turbulence on plankton predation strategies. *J. Theor. Biol.* **210**: 347–365. doi:10.1006/jtbi.2001.2310.
- Liberzon, A., B. Lüthi, M. Holzner, S. Ott, J. Berg, and J. Mann. 2012. On the structure of acceleration in turbulence. *Physica D* **241**: 208–215. doi:10.1016/j.physd.2011.07.008.
- MacKenzie, B. R., and T. Kjørboe. 1995. Encounter rates and swimming behavior of pause-travel and cruise larval fish predators in calm and turbulent laboratory environments. *Limnol. Oceanogr.* **40**: 1278–1289. doi:10.4319/lo.1995.40.7.1278.
- MacKenzie, B. R., and T. Kjørboe. 2000. Larval fish feeding and turbulence: A case for the downside. *Limnol. Oceanogr.* **45**: 1–10. doi:10.4319/lo.2000.45.1.0001.
- MacKenzie, B. R., T. J. Miller, S. Cyr, and W. C. Leggett. 1994. Evidence for a dome-shaped relationship between turbulence and larval fish ingestion rates. *Limnol. Oceanogr.* **39**: 1790–1799. doi:10.4319/lo.1994.39.8.1790.
- Mann, J., S. Ott, H. L. Pécseli, and J. Trulsen. 2003. Experimental studies of occupation times in turbulent flows. *Phys. Rev. E* **67**, 056307. doi:10.1103/PhysRevE.67.056307.
- Mann, J., S. Ott, H. L. Pécseli, and J. Trulsen. 2005. Turbulent particle flux to a perfectly absorbing surface. *J. Fluid Mech.* **534**: 1–21. doi:10.1017/S0022112005004672.
- Mann, J., S. Ott, H. L. Pécseli, and J. Trulsen. 2006. Laboratory studies of predator-prey encounters in turbulent environments: Effects of changes in orientation and field of view. *J. Plankton Res.* **28**: 509–522. doi:10.1093/plankt/fbi136.
- Osborn, T. 1996. The role of turbulent diffusion for copepods with feeding currents. *J. Plankton Res.* **18**: 185–195. doi:10.1093/plankt/18.2.185.
- Pécseli, H. L. 2000. *Fluctuations in Physical Systems*. Cambridge Univ. Press.
- Pécseli, H. L., and J. Trulsen. 2007. Turbulent particle fluxes to perfectly absorbing surfaces: A numerical study. *J. Turbul.* **8**, N42. doi:10.1080/14685240701615986.
- Pécseli, H. L., and J. Trulsen. 2010. Transit times in turbulent flows. *Phys. Rev. E* **81**, 046310. doi:10.1103/PhysRevE.81.046310.
- Pécseli, H. L., J. Trulsen, and Ø. Fiksen. 2010. Predator-prey encounter rates in turbulent water: Analytical models and numerical tests. *Prog. Oceanogr.* **85**: 171–179. doi:10.1016/j.pocean.2010.01.002.
- Pécseli, H. L., J. Trulsen, and Ø. Fiksen. 2012. Predator-prey encounter and capture rates for plankton in turbulent environments. *Prog. Oceanogr.* **101**: 14–32. doi:10.1016/j.pocean.2011.12.001.
- Rice, S. O. 1945. Mathematical analysis of random noise, II. *Bell System Tech. J.* **24–25**: Pp. 1–162. *Reprinted in* N. Wax [ed.], *Selected Papers on Noise and Stochastic Processes*. Pp. 133–294. Dover, 1954.
- Richardson, L. F. 1926. Atmospheric diffusion shown on a distance-neighbour graph. *Proc. R. Soc. Lond. A* **110**: 709–737. doi:10.1098/rspa.1926.0043.
- Rollefson, J. P. 1978. On Kolmogorov's theory of turbulence and intermittency. *Can. J. Phys.* **56**: 1426–1441. doi:10.1139/p78-190.
- Rothschild, B. J., and T. R. Osborn. 1988. Small-scale turbulence and plankton contact rates. *J. Plankton Res.* **10**: 465–474. doi:10.1093/plankt/10.3.465.
- Saiz, E., and M. Alcaraz. 1991. Effects of small-scale turbulence on development time and growth of *Acartia grani* (Copepoda: Calanoida). *J. Plankton Res.* **13**: 873–883. doi:10.1093/plankt/13.4.873.
- Saiz, E., and M. Alcaraz. 1992a. Enhanced excretion rates induced by small-scale turbulence in *Acartia* (Copepoda: Calanoida). *J. Plankton Res.* **14**: 681–689. doi:10.1093/plankt/14.5.681.
- Saiz, E., and M. Alcaraz. 1992b. Free-swimming behaviour of *Acartia clausi* (Copepoda: Calanoida) under turbulent water movement. *Mar. Ecol. Prog. Ser.* **80**: 229–236. doi:10.3354/meps080229.
- Saiz, E., and T. Kjørboe. 1995. Predatory and suspension-feeding of the copepod *Acartia-tonsa* in turbulent environments. *Mar. Ecol. Prog. Ser.* **122**: 147–158. doi:10.3354/meps122147.

- Schroeder, D. V. 2000. *An Introduction to Thermal Physics*. Addison Wesley Longman.
- Sundby, S., and P. Fossum. 1990. Feeding conditions of arcto-Norwegian cod larvae compared with the Rothschild-Osborn theory on small-scale turbulence and plankton contact rates. *J. Plankton Res.* **12**: 1153–1162. doi:10.1093/plankt/12.6.1153.
- Svensen, C., and T. Kiørboe. 2000. Remote prey detection in *Oithona similis*: Hydromechanical versus chemical cues. *J. Plankton Res.* **22**: 1155–1166. doi:10.1093/plankt/22.6.1155.
- Tennekes, H. 1968. Simple model for the small-scale structure of turbulence. *Phys. Fluids* **11**: 669–671. doi:10.1063/1.1691966.
- Tennekes, H. 1973. Intermittency of the small-scale structure of atmospheric turbulence. *Boundary-Layer Meteorol.* **4**: 241–250. doi:10.1007/BF02265235.
- Tsinober, A., P. Vedula, and P. K. Yeung. 2001. Random Taylor hypothesis and the behavior of local and convective accelerations in isotropic turbulence. *Phys. Fluids* **13**: 1974–1984. doi:10.1063/1.1375143.
- Urtizberea, A., and Ø. Fiksen. 2013. Effects of prey size structure and turbulence on feeding and growth of anchovy larvae. *Environ. Biol. Fishes* **96**: 1045–1063. doi:10.1007/s10641-012-0102-6.
- Visser, A. W. 2001. Hydromechanical signals in the plankton. *Mar. Ecol. Prog. Ser.* **222**: 1–24. doi:10.3354/meps222001.
- Visser, A. W., and T. Kiørboe. 2006. Plankton motility patterns and encounter rates. *Oecologia* **148**: 538–546. doi:10.1007/s00442-006-0385-4.
- Visser, A. W., P. Mariani, and S. Pigolotti. 2009. Swimming in turbulence: Zooplankton fitness in terms of foraging efficiency and predation risk. *J. Plankton Res.* **31**: 121–133. doi:10.1093/plankt/fbn109.
- Visser, A. W., H. Saito, E. Saiz, and T. Kiørboe. 2001. Observations of copepod feeding and vertical distribution under natural turbulent conditions in the North Sea. *Mar. Biol.* **138**: 1011–1019. doi:10.1007/s002270000520.
- Yen, J., P. H. Lenz, D. V. Gassie, and D. K. Hartline. 1992. Mechanoreception in marine copepods: Electrophysiological studies on the first antennae. *J. Plankton Res.* **14**: 495–512. doi:10.1093/plankt/14.4.495.
- Zilman, G., J. Novak, A. Liberzon, S. Perkol-Finkel, and Y. Benayahu. 2013. The hydrodynamics of contact of a marine larva, *Bugula neritina*, with a cylinder. *J. Exp. Biol.* **216**: 2789–2797. doi:10.1242/jeb.083352.

Received: 9 July 2013

Amended: 19 February 2014

Accepted: 10 April 2014